The Ionic Track in the F_1-ATPase from the Thermophilic *Bacillus* PS3[†]

Sanjay Bandyopadhyay and William S. Allison*

Department of Chemistry & Biochemistry, University of California at San Diego, La Jolla, California 92093-0601

Received November 17, 2003; Revised Manuscript Received January 12, 2004

ABSTRACT: Only $\beta-\beta$ cross-links form when the $\alpha_3(\beta E^{395}C)_3\gamma K^{36}C$ (MF_1 residue numbers) double mutant subcomplex of TF_1, the F_1-ATPase from the thermophilic *Bacillus* PS3, is slowly inactivated with $CuCl_2$ in the presence or absence of MgATP. The same slow rate of inactivation and extent of $\beta-\beta$ cross-linking occur upon treatment of the $\alpha_3(\beta E^{395}C)_3\gamma$ single mutant subcomplex with $CuCl_2$ under the same conditions. In contrast, the $\alpha_3(\beta E^{395}C)_3\gamma R^{33}C$ and $\alpha_3(\beta E^{395}C)_3\gamma R^{75}C$ double mutant subcomplexes of TF_1 are rapidly inactivated by $CuCl_2$ under the same conditions that is accompanied by complete $\beta-\gamma$ cross-linking. The ATPase activity of each mutant enzyme containing the $\beta E^{395}C$ substitution is stimulated to a much greater extent by the nonionic detergent lauryldimethylamine oxide (LDAO) than wild-type enzyme, whereas the ATPase activities of the $\gamma R^{33}C$, $\gamma K^{36}C$, and $\gamma R^{75}C$ single mutants are stimulated to about the same extent as wild-type enzyme by LDAO. This indicates that the $E^{395}C$ substitution in the ^{394}DELSEED^{400} segment of β subunits increases propensity of the enzyme to entrap inhibitory MgADP in a catalytic site during turnover. These results are discussed in perspective with (i) the ionic track predicted from molecular dynamics simulations to operate during energy-driven ATP synthesis by MF_1, the F_1-ATPase from bovine heart mitochondria [Ma, J., Flynn, T. C., Cui, Q., Leslie, A. G. W., Walker, J. E., and Karplus, M. (2002) *Structure 10*, 921−931]; and (ii) the possibility that the $\beta E^{395}C$ substitution might induce a global effect that alters affinity of noncatalytic sites for nucleotides or alters communication between noncatalytic sites and catalytic sites during ATP hydrolysis.

When dissociated from the membrane in soluble form, the F_1 component of the F_oF_1-ATP synthases found in energy transducing membranes is an ATPase comprised of five different subunits in $\alpha_3\beta_3\gamma\delta\epsilon$ stoichiometry. F_1-ATPases contain six nucleotide binding sites. Three are catalytic sites that are located mostly on β subunits at α/β interfaces and contain at least one amino acid side chain derived from adjacent α subunits. Noncatalytic nucleotide binding sites, which do not have a well-defined functional role, are located mostly on α subunits at other α/β interfaces (*1*).

In crystal structures of bovine heart mitochondria F_1-ATPase (MF_1)[1] (*2*−*5*), the α and β subunits are elongated and interact in an alternating, hexameric array surrounding a coiled-coil made up of the α-helical N- and C-termini of the γ subunit. In the original crystal structure (*2*), noncatalytic sites are homogeneously liganded with Mg-5′-adenylyl-β,γ-imidophosphate (MgAMP-PNP), and α subunits are present in closed conformations, whereas catalytic sites are heterogeneously liganded. Two β subunits are in closed conformations. One, designated β_{TP}, contains MgAMP-PNP bound to the catalytic site and another, designated β_{DP}, contains MgADP bound to the catalytic site. The third β subunit, designated β_E, is in an open conformation with an empty catalytic site. Amino acid side chains that interact with anionic oxygens of nucleotides or the Mg^{2+} ion complexed with anionic oxygens of bound nucleotides are arranged similarly in catalytic sites of β_{TP} and β_{DP} that have closed conformations, but are arranged very differently in the catalytic site of β_E that has an open conformation.

Single molecule experiments pioneered by the collaborative efforts of the Yoshida and Kinosita laboratories, designed on the basis of the original crystal structure of MF_1 (*2*), have shown that sequential firing of the three catalytic sites of F_1 during ATP hydrolysis is coupled to counterclockwise rotation of the γ subunit in distinct 120° steps as ATP is hydrolyzed (*6*−*8*). However, the precise molecular events that couple ATP synthesis and hydrolysis at catalytic sites to rotation of the γ subunit have not been elucidated. The crystal structures of MF_1 have provided the rationale for probing the molecular mechanism of ATP synthase using mutational analysis and molecular dynamics simulations as tools.

In the crystal structure of MF_1 deduced by Gibbons et al. (*4*), in which the carboxylate of E^{199} in β_{DP} is derivatized with *N*,*N*′-dicyclohexylcarbodiimide (DCCD-MF_1), the guanidinium of γArg^{36} is near the carboxylate of $\beta_E Glu^{395}$.[2] When the $\alpha_3(\beta E^{395}C)_3\gamma K^{36}C$ double mutant subcomplex of TF_1, the F_1-ATPase from the thermophilic *Bacillus* PS3, was treated

[†] This work was supported by NIGMS Grant GM 16974 from the National Institutes of Health.

* To whom correspondence should be addressed. Tel.: 858-534-3057. Fax: 858-822-0079. E-mail: wsa@checfs2.ucsd.edu.

[1] Abbreviations: MF_1, TF_1, EF_1, CF_1; the F_1-ATPases from bovine heart mitochondria, the thermophilic *Bacillus* PS3, *Escherichia coli* and chloroplasts, respectively; AMP-PNP, 5′-adenylyl-β,γ-imidophosphate; LDAO, lauryldimethylamine oxide; DTT, dithiothreitol; DCCD, *N*,*N*′-dicyclohexylcarbodiimide; *cm*C, *S*-carboxymethyl cysteine.

[2] Unless stated otherwise, residue numbers of MF_1 are used throughout. In MF_1, βE^{395} is equivalent to βE^{391} of TF_1; γR^{36} of MF_1 is equivalent to γK^{36} of TF_1, γR^{33} in MF_1 is equivalent to γR^{33} in TF_1, and γR^{75} of MF_1 is equivalent to γR^{83} in TF_1.

10.1021/bi036058i CCC: $27.50
Published on Web 02/12/2004

with $CuCl_2$, $\beta-\gamma$ cross-linking was not observed. However, slow $\beta-\beta$ cross-linking was observed that was accompanied by inactivation of ATPase activity (unpublished experiments, 2000). Subsequently, Ma et al. (*9*) proposed, on the basis of molecular dynamics simulations using coordinates from crystal structures of MF_1, that the guanidinium of γArg^{36} is part of an ionic track that guides sequential closing and opening of β subunits coupled to energy-driven, clockwise rotation of the γ subunit during ATP synthesis. According to the simulations, the coiled coil comprised of amino- and carboxyl-terminal α-helices of the γ subunit undergoes unwinding and rewinding during each 120° rotational step of ATP synthesis that drives the $\beta_{TP} \rightarrow \beta_E$, $\beta_E \rightarrow \beta_{DP}$, and $\beta_{DP} \rightarrow \beta_{TP}$ interconversions. Their model suggests that the trajectory of the rotating γ subunit is guided by electrostatic interactions between positively charged side chains in the γ subunit and negatively charged side chains in the turn of the helix−turn−helix motif in the C-terminal domains of β subunits (the ^{392}GMDELS^{397} segments). As pointed out by Ma et al. (*9*), only 6 of the 18 Lys or Arg residues in the γ subunit that are postulated to comprise the ionic track in MF_1 are highly conserved. Whereas positively charged side chains in position 36 are poorly conserved, those in positions 33 and 75 are highly conserved in the over 70 sequences of the γ subunit obtained from searching Swiss-Prot/TrEMBL and GenBank.

Given that $\beta-\gamma$ cross-links were not formed when the $\alpha_3(\beta E^{395}C)_3\gamma K^{36}C$ subcomplex was treated with $CuCl_2$ implies that γLys^{36} of TF_1 might not function in an ionic track analogous to that proposed for MF_1. To test whether γArg^{33} and γArg^{75} in TF_1 might be part of an ionic track analogous to the one described by Ma et al. in MF_1 (*9*), the $\alpha_3(\beta E^{395}C)_3\gamma R^{33}C$ and $\alpha_3(\beta E^{395}C)_3\gamma(R^{75}C)$ mutant subcomplexes of TF_1 have been prepared and characterized before and after treatment with $CuCl_2$. The results of these characterizations as well as the characteristics of inactivation of the $\alpha_3(\beta E^{395}C)_3\gamma$ and $\alpha_3(\beta E^{395}C)_3\gamma(K^{36}C)$ mutant subcomplexes of TF_1 with $CuCl_2$ are presented and discussed in this report.

EXPERIMENTAL PROCEDURES

Generation and Expression of Mutant Plasmids. The expression plasmid pKK encoding the α, β, and γ subunits of TF_1 was used for both site-directed mutagenesis and gene expression (*10*). Site specific mutations in the wild-type pKK expression plasmid were performed by polymerase chain reactions using the QuikChange site-directed mutagenesis kit from Stratagene. The mutagenic oligonucleotides along with their corresponding complements (not shown) that were used to incorporate the $\alpha_3(\beta E^{395}C)_3\gamma$, $\alpha_3\beta_3\gamma R^{33}C$, $\alpha_3\beta_3\gamma K^{36}C$, and $\alpha_3\beta_3\gamma R^{75}C$ single mutations into the wild-type expression plasmid are 5′-GGGGATGGATTGCCTGTCGGATGAAG-3′, 5′-CGAAGCTGAACTGTGCGGAGCAAAACG-3′, 5′-CGCGCGGAGCATGTCGCGAAATCG-3′, and 5′-CACGT-CGGATTGCGGTCTGGCTGG-3′, respectively. The bases changed are underlined. For generation of the $\alpha_3(\beta E^{395}C)_3\gamma R^{33}C$, $\alpha_3(\beta E^{395}C)_3\gamma K^{36}C$, and $\alpha_3(\beta E^{395}C)_3\gamma R^{75}C$ double mutant subcomplexes, pKK plasmid DNA containing the $\beta E^{395}C$ single mutation was used as template. The wild-type and mutant plasmids were purified using the Wizard Plus miniprep kit from Promega. Introduction of each mutation was confirmed by DNA sequencing. The mutant plasmids were expressed in *Escherichia coli* strain JM103 (*unc*$^-$). Purification of the wild-type $\alpha_3\beta_3\gamma$ and mutant subcomplexes were carried out as described previously and stored as precipitates in 75% saturated ammonium sulfate at 4 °C (*10*).

Analytical Methods. The isolated wild type and mutant $\alpha_3\beta_3\gamma$ subcomplexes, at 1 mg/mL in 50 mM Tris-Cl buffer, pH 8.0 were treated with 10 mM CDTA for 15 min at 23 °C, at which time 100 μL aliquots were passed through 1-mL centrifuge columns of Sephadex G-50 equilibrated with the same buffer containing 0.1 mM EDTA. The enzyme subcomplexes obtained by this treatment were essentially free from endogenous bound nucleotides as assessed by anion exchange HPLC as described previously (*11*).

ATPase activity was determined spectrophotometrically in the presence of 2 mM ATP and 3 mM Mg^{2+} at pH 8.0 and 30 °C using an ATP regeneration system coupled to oxidation of NADH, which was monitored at 340 nm with a Uvikon-XL double beam spectrophotometer. Traces were recorded within 3 s after initiating the reactions by injecting small volumes of enzyme solutions into 1 mL of rapidly stirred assay medium. Protein concentrations were determined by the method of Bradford using Coomassie Blue from Pierce (*12*).

Oxidation of the Reduced $\alpha_3(\beta E^{395}C)_3\gamma$ Single and $\alpha_3(\beta E^{395}C)_3\gamma R^{33}C$, $\alpha_3(\beta E^{395}C)_3\gamma K^{36}C$, and $\alpha_3(\beta E^{395}C)_3\gamma R^{75}C$ Double Mutant Subcomplexes with $CuCl_2$. Prior to oxidation with $CuCl_2$, the single and double mutants containing the $\beta E^{395}C$ substitution were reduced with 10 mM dithiothreitol (DTT) in 50 mM Tris-Cl, pH 8.0 containing 0.1 mM EDTA for 1 h, at which time excess DTT and EDTA were removed by passing samples through centrifuge columns of Sephadex G-50 equilibrated with 50 mM Tris-Cl, pH 8.0 (*13*). Unless stated otherwise, oxidation of the fully reduced single or double mutants, at 1 mg/mL in 50 mM Tris-Cl, pH 8.0 was carried out with 100 μM $CuCl_2$ at 23 °C. After complete oxidation of the sample, excess $CuCl_2$ was removed by passing 100 μL aliquots of oxidized protein samples through 1-mL centrifuge columns of Sephadex G-50 equilibrated with 50 mM Tris-Cl, pH 8.0.

Analysis of Cross-Linking by SDS−PAGE after Treatment of the Double Mutants with $CuCl_2$. Samples containing 6 μg of the reduced or oxidized single and double mutants were diluted 1:4 with SDS−PAGE sample buffer containing 62.5 mM Tris-Cl, pH 6.8, 10% glycerol, 0.025% bromophenol blue, and 2% SDS. After application of the denatured samples, the 12% Tris-Cl Ready Gels from Bio-Rad were submitted to electrophoresis at 200 V for 40 min. After staining with 0.1% Coomassie Brilliant Blue R-250 followed by thorough destaining, the gels were photographed with a Polaroid camera. The photographs were scanned with an EPSON Perfection 1250 scanner, and the extent of cross-linking was quantified with GelExpert software from Nucleotech.

Carboxymethylation of the Reduced $\alpha_3(\beta E^{395}C)_3\gamma$ Single Mutant Subcomplex. The fully reduced $\beta E^{395}C$ single mutant, at 1 mg/mL in 50 mM Tris-Cl, pH 8.0 containing 0.1 mM EDTA was treated for 20 h at 23 °C with 4 mM iodo[^{3}H]-acetate (American Radiolabeled Chemicals) adjusted to pH 7.0 with NaOH. Excess iodo[^{3}H]acetate was removed by passing 100 μL solutions of the reaction mixtures through 1-mL centrifuge columns of Sephadex G-50 equilibrated with 50 mM Tris-Cl, pH 8.0. Radioactivity was determined by

Table 1: Nearest Distances between the Guanidiniums of γArg^{36}, γArg^{33}, and γArg^{75} and the Carboxylate of βGlu^{395} in Crystal Structures of Bovine MF_1

crystal structure	γR^{36}-$\beta_E E^{395}$	γR^{33}-$\beta_E E^{395}$	γR^{75}-$\beta_{DP} E^{395}$
DCCD-MF_1 (4)	4.26 Å	9.56 Å	3.15 Å
original MF_1 (2)	11.02	18.03	
$(AlF_3)_2$-MF_1 (3)	9.95	18.29	
$(AlF_4^-)_2$-MF_1 (5)	6.32	3.13	3.27

Table 2: Steady State ATPase Activities of the Wild-Type and Mutant $\alpha_3\beta_3\gamma$ Subcomplexes

subcomplex	specific activity[a]
$\alpha_3\beta_3\gamma$	20 μmol of ATP mg^{-1} min^{-1}
$\alpha_3(\beta E^{395}C)_3\gamma$	0.9
$\alpha_3(\beta E^{395}C)_3(\gamma R^{33}C)$	0.3
$\alpha_3(\beta E^{395}C)_3(\gamma K^{36}C)$	0.6
$\alpha_3(\beta E^{395}C)_3(\gamma R^{75}C)$	1.6
$\alpha_3\beta_3(\gamma R^{33}C)$	16
$\alpha_3\beta_3(\gamma K^{36}C)$	17
$\alpha_3\beta_3(\gamma R^{75}C)$	25

[a] The specific activities represent the final steady-state rate observed for the hydrolysis of 2 mM ATP using the ATP regeneration system containing 2 mM ATP, 3 mM $MgCl_2$, 0.25 mM NADH, 20 units of pyruvate kinase, and 10 units of lactate dehydrogenase in 50 mM Hepes-KOH, pH 8.0.

liquid scintillation counting using Ecoscint from National Diagnostics.

RESULTS

Only $\beta-\beta$ Cross-Links Form upon Treatment of the $\alpha_3(\beta E^{395}C)_3\gamma K^{36}C$ Double Mutant Subcomplex with $CuCl_2$. Table 1 summarizes the nearest distances between one of the guanidinium nitrogens in the side chains of γArg^{33}, γArg^{36}, and γArg^{75} and one of the carboxylate oxygens of βGlu^{395} in crystal structures of MF_1. In the crystal structure of MF_1 containing Glu^{199} in β_{DP} derivatized with DCCD (DCCD-MF_1) (*4*), one of the guanidinium nitrogens of γR^{36} is 4.3 Å from a carboxylate oxygen of E^{395} in β_E. In the crystal structure containing MgADP-fluoroaluminate complexes in two closed β subunits and MgADP in half closed β_E ($(AlF_4^-)_2$-MF_1) (*5*), a carboxylate oxygen of E^{395} in half-closed β_E is 3.13 Å from one of the guanidinium nitrogens of γR^{33}. In all other crystal structures of MF_1, including those not represented in Table 1, the carboxylate oxygens in the side chain of βGlu^{395} in all three β subunits are at least 10 Å from a guanidinium nitrogen in the side chains of γArg^{33} and γArg^{36}. With the exception of the DCCD-MF_1 and $(AlF_4^-)_2$-MF_1 crystal structures, the region of the γ subunit containing γR^{75} is not sufficiently ordered to reveal the guanidinium side chain. In the two crystal structures containing the complete γ subunit, a guanidinium nitrogen of γR^{75} is about 3.2 Å from a carboxylate oxygen of E^{395} in β_E.

The steady-state ATPase activities of the wild type and mutant $\alpha_3\beta_3\gamma$ subcomplexes characterized in this study are compared in Table 2. The specific activity of each mutant subcomplex containing the $\beta E^{395}C$ substitution is less than 10% that of the wild-type subcomplex. In contrast, the specific activities of the subcomplexes containing the $\gamma R^{33}C$, $\gamma K^{36}C$, and $\gamma R^{75}C$ single substitutions are in the same range as the specific activity of the wild-type subcomplex.

Figure 1 illustrates the rates of inactivation of the fully reduced $\beta E^{395}C$ single mutant and the fully reduced $\beta E^{395}C/\gamma K^{36}C$ double mutant by 500 μM $CuCl_2$ in the presence and absence of 1 mM MgATP. In the absence of nucleotides, treatment of the $\beta E^{395}C$ single mutant with $CuCl_2$ led to slow inactivation of ATPase activity that leveled at about 70% inactivation after 2 h (closed circles). Further inactivation was not observed after 18 h. In the presence of 1 mM MgATP, the $\beta E^{395}C$ single mutant was inactivated somewhat more slowly by 500 μM $CuCl_2$ than observed in the absence of MgATP (closed triangles). Treatment of the reduced $\beta E^{395}C$ single mutant subcomplex with 1 mM MgATP in the absence of $CuCl_2$ and DTT had no effect on ATPase activity (closed squares).

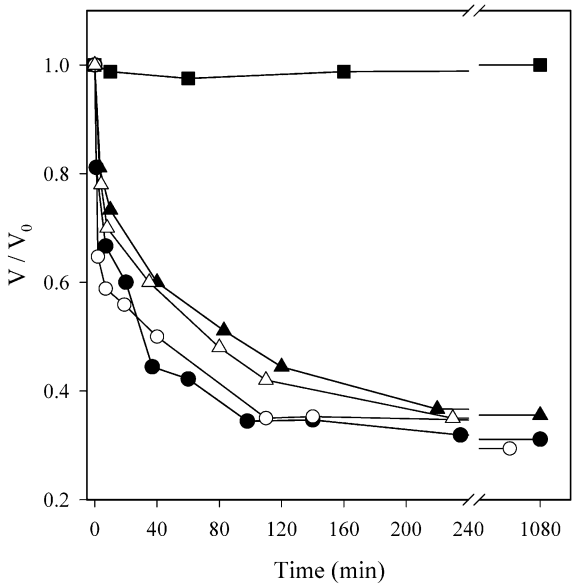

FIGURE 1: Rates of inactivation of the $\alpha_3(\beta E^{395}C)_3\gamma$ single and $\alpha_3(\beta E^{395}C)_3\gamma K^{36}C$ double mutant subcomplexes by $CuCl_2$ in the presence and absence of MgATP. The completely reduced $\beta E^{395}C$ single and $\beta E^{395}C/\gamma K^{36}C$ double mutants were prepared as described under Experimental Procedures. Immediately before addition of $CuCl_2$, excess DTT and EDTA were removed from the reduced enzyme solutions by passing 100 μL aliquots through 1-mL centrifuge columns of Sephadex G-50 equilibrated with 50 mM Tris-Cl, pH 8.0. The reduced single and double mutant subcomplexes prepared in this manner were incubated at 1 mg/mL with the following additions before assaying 10 μL samples for ATPase activity at the times indicated: $\alpha_3(\beta E^{395}C)_3\gamma$ plus 1 mM MgATP (closed squares); $\alpha_3(\beta E^{395}C)_3\gamma$ plus 500 μM $CuCl_2$ (closed circles); $\alpha_3(\beta E^{395}C)_3\gamma$ plus 1 mM MgATP and 500 μM $CuCl_2$ (closed triangles); $\alpha_3(\beta E^{395}C)_3\gamma K^{36}C$ plus 500 μM $CuCl_2$, (open circles); $\alpha_3(\beta E^{395}C)_3\gamma K^{36}C$ with 1 mM MgATP plus 500 μM $CuCl_2$ (open triangles).

Figure 1 also illustrates that the reduced $\beta E^{395}C/\gamma K^{36}C$ double mutant exhibited essentially same rate and extent of inactivation as the $\beta E^{395}C$ single mutant when treated with 500 μM $CuCl_2$ in the presence (open triangles), or absence of 1 mM MgATP (open circles). No loss of activity was observed when the reduced double mutant was incubated with or without added MgATP for 18 h in the absence of $CuCl_2$ and DTT.

Figure 2 shows that substantial $\beta-\beta$ cross-linking was observed when samples of the single and double mutants that had been inactivated for 2 h with $CuCl_2$ in the presence and absence of MgATP were submitted to SDS−PAGE. The distributions of cross-linked and non-cross-linked β subunits are essentially the same in the gels representing the $\alpha_3(\beta E^{395}C)_3\gamma$ and $\alpha_3(\beta E^{395}C)_3\gamma K^{36}C$ subcomplexes after inac-

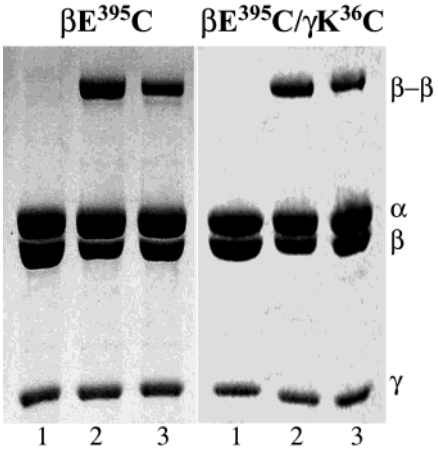

FIGURE 2: The cross-linked species resolved by SDS−PAGE after inactivation of the $\alpha_3(\beta E^{395}C)_3\gamma$ and $\alpha_3(\beta E^{395}C)_3\gamma K^{36}C$ mutant subcomplexes with $CuCl_2$ in the presence and absence of MgATP. Samples, 7 μg each, were withdrawn after incubating the reaction mixtures described in the legend of Figure 1 for 2 h at 23 °C. The samples were submitted to SDS−PAGE as described under Experimental Procedures. The samples in the gel illustrated for the $\alpha_3(\beta E^{395}C)_3\gamma$ single mutant contained: (lane 1) enzyme plus 10 mM DTT; (lane 2) enzyme plus 500 μM $CuCl_2$; and (lane 3) enzyme plus 1 mM MgATP followed by 500 μM Cu^{2+}. The samples in the gel illustrated for the $\alpha_3(\beta E^{395}C)_3\gamma K^{36}C$ double mutant contained: (lane 1) enzyme plus 10 mM DTT; (lane 2) enzyme plus 500 μM Cu^{2+}; (lane 3) enzyme plus 1 mM MgATP followed by 500 μM Cu^{2+}.

tivation for 2 h with $CuCl_2$ in the presence or absence of MgATP. It is clear that $\beta-\gamma$ cross-links were not formed when the double mutant enzyme was maximally inactivated by $CuCl_2$ in the presence or absence of MgATP. Analysis of the band intensities in the gel illustrated in Figure 2, as described under Experimental Procedures, revealed that oxidation of the reduced $\beta E^{395}C$ single mutant by 500 μM Cu^{2+} led to about 1.5 mol of $\beta-\beta$ cross-links per mol of the single mutant subcomplex. This represents about 75% cross-linking of two β subunits as shown in lane 2, whereas oxidation of the reduced enzyme in the presence of 1 mM MgATP resulted in 65% cross-linking of the two closed β subunits, under the same conditions, as shown in lane 3 of Figure 2 illustrated for the $\beta E^{395}C$ single mutant. On the other hand, lanes 2 and 3 of Figure 2 illustrated for the $\beta E^{395}C/\gamma K^{36}C$ double mutant show that oxidation of the reduced $\beta E^{395}C/\gamma K^{36}C$ double mutant by 500 μM $CuCl_2$ in the absence and presence of 1 mM MgATP, respectively, led to about 65% cross-linking of the two closed β subunits.

Predominant $\beta-\gamma$ Cross-Linking Accompanies Rapid Inactivation of the $\alpha_3(\beta E^{395}C)_3\gamma R^{33}C$ and $\alpha_3(\beta E^{395}C)_3\gamma R^{75}C$ Double Mutant Subcomplexes with $CuCl_2$. Treatment of the $\alpha_3(\beta E^{395}C)_3\gamma R^{33}C$ and $\alpha_3(\beta E^{395}C)_3\gamma R^{75}C$ mutant subcomplexes with 100 μM $CuCl_2$ in the presence or absence of 1 mM MgATP led to greater than 95% inactivation of ATPase activity within 2 min. Figure 3 illustrates the cross-linking patterns obtained after submitting samples of the reaction mixtures that were withdrawn 30 min after introducing $CuCl_2$ to SDS−PAGE. In each case, all or nearly all of the γ subunit was cross-linked to a β subunit, indicating that $\beta-\gamma$ cross-linking was responsible for the rapid inactivation observed. Treatment of the double mutants with $CuCl_2$ led to a minor $\beta-\beta$ cross-linking that probably occurred after $\beta-\gamma$ cross-linking was complete.

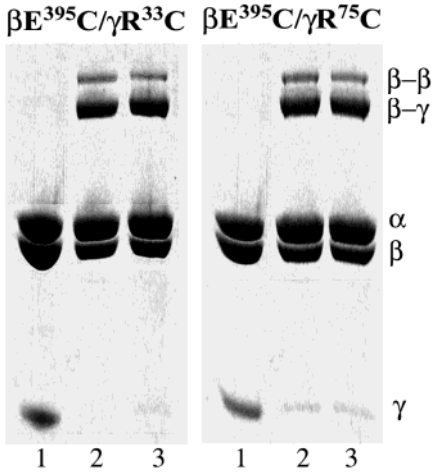

FIGURE 3: The cross-linked species resolved upon submission of the $CuCl_2$-inactivated $\alpha_3(\beta E^{395}C)_3\gamma R^{33}C$ and $\alpha_3(\beta E^{395}C)_3\gamma R^{75}C$ double mutant subcomplexes to SDS−PAGE. Samples containing 7 μg each of the reduced double mutants were submitted to SDS−PAGE before and after treatment with 100 μM $CuCl_2$ for 30 min at 23 °C in the presence and absence of 1 mM MgATP. The samples in the gel illustrated for the $\alpha_3(\beta E^{395}C)_3\gamma R^{33}C$ double mutant contained: (lane 1) enzyme plus 10 mM DTT; (lane 2) enzyme plus 100 μM $CuCl_2$; (lane 3) enzyme plus 1 mM MgATP followed by 100 μM $CuCl_2$. The samples in the gel illustrated for the $\alpha_3(\beta E^{395}C)_3\gamma R^{75}C$ double mutant contained: (lane 1) enzyme plus 10 mM DTT; (lane 2) enzyme plus 100 μM $CuCl_2$; (lane 3) enzyme plus 1 mM MgATP followed by 100 μM $CuCl_2$.

The $\beta E^{395}C$ Substitution Increases Propensity to Entrap Inhibitory MgADP in a Catalytic Site during Turnover. The wild-type $\alpha_3\beta_3\gamma$ subcomplex of TF_1 has high propensity to entrap inhibitory MgADP in a catalytic site during turnover (*14*, *15*). As shown in Figure 4, hydrolysis of 2 mM ATP by the wild-type subcomplex was stimulated about 4-fold in the presence of lauryldimethylamine oxide (LDAO), which prevents entrapment of inhibitory MgADP in a catalytic site. Entrapment of inhibitory MgADP was provoked in the presence of azide, which increases the affinity of inhibitory MgADP at the affected catalytic site, presumably by liganding to the Mg^{2+} ion (*11*). In contrast, the $\alpha_3(\beta E^{395}C)_3\gamma$ single mutant hydrolyzed 2 mM ATP with pronounced deceleration over the initial 30 s that decreased to a final rate that was 4.5% the rate exhibited by the wild-type enzyme. This indicates that the single mutant subcomplex has much higher propensity than the wild-type enzyme to entrap inhibitory MgADP in a catalytic site during turnover. This is consistent with the finding that LDAO stimulates the hydrolysis of 2 mM ATP by the single mutant enzyme 11-fold, whereas the ATPase activity of the wild-type enzyme is stimulated only 4.3-fold by LDAO under the same conditions.

Figure 4 also shows that each double mutant containing the $\beta E^{395}C$ substitution has higher propensity than the wild-type enzyme to entrap inhibitory MgADP in a catalytic site during turnover. Similar to the single mutant, all three double mutants exhibit rapid deceleration from the initial rate when 2 mM ATP was hydrolyzed in the absence of additions. In the presence of LDAO, the steady-state rates of hydrolysis of 2 mM ATP by the $\alpha_3(\beta E^{395}C)_3\gamma K^{36}C$, $\alpha_3(\beta E^{395}C)_3\gamma R^{33}C$, and $\alpha_3(\beta E^{395}C)_3\gamma R^{75}C$ double mutants are 7-, 25-, and 12.5-fold greater, respectively, than the steady-state rates recorded in the absence of additions.

The Propensity of the $\alpha_3\beta_3\gamma K^{36}C$, $\alpha_3\beta_3\gamma R^{33}C$, and $\alpha_3\beta_3\gamma R^{75}C$ Single Mutants to Entrap Inhibitory MgADP in

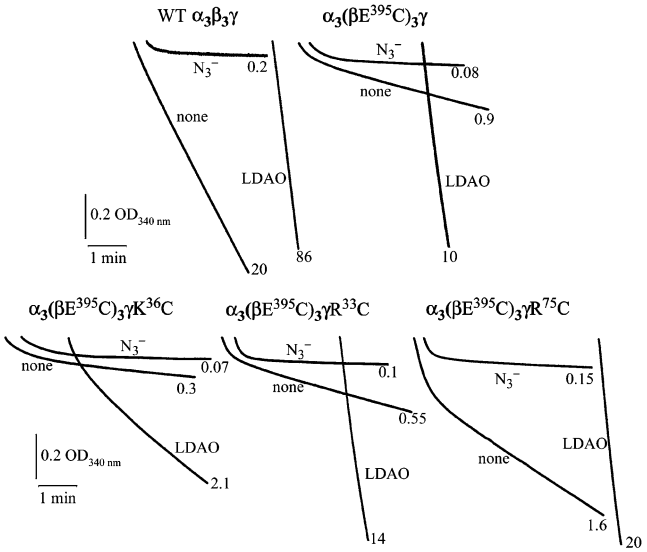

FIGURE 4: Comparison of the effects of NaN_3 and LDAO on hydrolysis of 2 mM ATP by the wild-type $\alpha_3\beta_3\gamma$ and reduced mutant subcomplexes containing the $\beta E^{395}C$ substitution. Assays were initiated by injecting 2 μg of the wild-type or 10 μg of the reduced $\beta E^{395}C$ single and $\beta E^{395}C/\gamma K^{36}C$, $\beta E^{395}C/\gamma R^{33}C$, and $\beta E^{395}C/\gamma R^{75}C$ double mutants into 1 mL of rapidly stirred assay medium containing 20 U/mL pyruvate kinase, 10 U/mL lactate dehydrogenase, 30 mM KCl, 4 mM phosphoenolpyruvate, 0.25 mM NADH, 2 mM ATP and 3 mM $MgCl_2$ in 50 mM Hepes-KOH, pH 8.0 in the presence and absence of 1 mM NaN_3 or 0.06% LDAO. Traces were initiated within 3 s after injecting the samples. The numbers on the traces represent the final rates of ATP hydrolysis recorded in the last 30 s of each assay expressed in μmol of ATP hydrolyzed mg^{-1} min^{-1}.

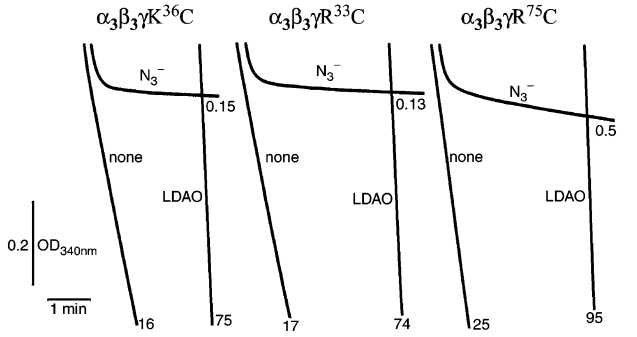

FIGURE 5: Comparison of the effects of LDAO and NaN_3 on hydrolysis of 2 mM ATP by the $\alpha_3\beta_3\gamma K^{36}C$, $\alpha_3\beta_3\gamma R^{33}C$ and $\alpha_3\beta_3\gamma R^{75}C$ single mutant subcomplexes. Assays were performed as described in the legend of Figure 4 using 5 μg of the $\gamma K^{36}C$, $\gamma R^{33}C$, or $\gamma R^{75}C$ single mutant in the presence and absence of 1 mM NaN_3 or 0.06% LDAO. The numbers on the traces represent the final rates of ATP hydrolysis recorded in the last 30 s of each assay expressed in μmol of ATP hydrolyzed mg^{-1} min^{-1}.

a Catalytic Site During Turnover Is Comparable to that of Wild-Type Enzyme. Figure 5 shows that in the absence of additions, the $\alpha_3\beta_3\gamma K^{36}C$, $\alpha_3\beta_3\gamma R^{33}C$, and $\alpha_3\beta_3\gamma R^{75}C$ single mutant subcomplexes hydrolyze 2 mM ATP with specific activities of 16, 17, and 25 μmol mg^{-1} min^{-1} in the absence of additions. These specific activities are comparable to the specific activity of the wild-type enzyme under the same conditions. Like the wild-type enzyme, each single mutant enzyme exhibits rapid, turnover-dependent inactivation in the presence of 1 mM NaN_3. The ATPase activities of the single mutants containing the $\gamma K^{36}C$, $\gamma R^{33}C$, and $\gamma R^{75}C$ substitutions were stimulated 4.7-, 4.4-, and 3.8-fold, respectively, by LDAO. These activations are comparable to the 4.3-fold stimulation of the ATPase activity of the wild-type enzyme induced by LDAO illustrated in Figure 4.

Carboxymethylation of the Introduced Cysteines Increases the ATPase Activity of the $\alpha_3(\beta E^{395}C)_3\gamma$ Mutant 2-Fold. Tsunoda et al. (*16*) pointed out that the side chains of Ile^{390} in β_{DP} and β_{TP} are in van der Waals contact in crystal structures of MF_1. The carboxylates of E^{395} are about 8.5 Å apart at the β_{DP}/β_{TP} interface in crystal structures of MF_1 (*2*−*5*). This raises the possibility that electrostatic repulsion of the side chains of βE^{395} at the β_{DP}/β_{TP} interface might be important for optimal catalysis. To test this possibility, the $\alpha_3(\beta E^{395}C)_3\gamma$ mutant subcomplex was carboxymethylated with iodo[^{3}H]acetate. An earlier study showed that the naturally occurring cysteine in position-193 of the α subunit was not labeled after prolonged incubation of the wild-type subcomplex with iodo[^{3}H]acetate under the conditions described in the legend of Figure 6 (*17*). Therefore, it is probable that only the introduced cysteines were carboxymethylated when the $\alpha_3(\beta E^{395}C)_3\gamma$ mutant subcomplex was treated with the reagent. The ATPase activity of the mutant subcomplex responded in two phases when it was treated with iodo[^{3}H]acetate, as shown by the open circles in Figure 6A. About 40% inactivation occurred within 1 h after adding iodo[^{3}H]acetate to the reduced single mutant subcomplex at a final concentration of 4 mM. About 1 mol of [^{3}H]acetate was incorporated per mol of enzyme after 1 h. This was followed by slow reactivation of ATPase activity. Maximal reactivation was observed when about 3 mol of [^{3}H]acetate were incorporated per mol of enzyme. Figure 6A also illustrates that the initial, rapid inactivation phase was associated with derivatization of $Glu^{395}Cys$ in a single β subunit, whereas the slow reactivation phase was associated with derivatization of the introduced cysteines in the two other β subunits (closed squares). After 20 h, all three introduced cysteines were carboxymethylated. To explain the biphasic response of the ATPase activity to carboxymethylation, we propose that the inactivation phase was caused by asymmetry introduced when one or two of the introduced cysteines were carboxymethylated, whereas activation occurs when all three of the introduced cysteines were carboxymethylated.

Figure 6B illustrates the effects of NaN_3 and LDAO on hydrolysis of 2 mM ATP catalyzed after carboxymethylation of all three introduced cysteines in the $\alpha_3(\beta E^{395}C)_3\gamma$ mutant subcomplex (*cm*C-$\alpha_3(\beta E^{395}C)_3\gamma$). In the absence of additions, the completely carboxymethylated mutant enzyme hydrolyzed 2 mM ATP with a specific activity of 1.9 μmol of ATP hydrolyzed mg^{-1} min^{-1}. This is 10% of the rate exhibited by wild type and only twice the rate exhibited by the mutant subcomplex before carboxymethylation. In the presence of 1 mM NaN_3, ATP hydrolysis by the carboxymethylated $\beta E^{395}C$ was strongly inhibited in a turn-over-dependent manner and was stimulated 8-fold by 0.06% LDAO. Therefore, carboxymethylation of the introduced cysteines has only a minor stimulatory effect and does not reduce propensity to entrap inhibitory MgADP in a catalytic site during turnover.

DISCUSSION

Demonstration that only $\beta-\beta$ cross-links form upon inactivation of the $\beta E^{395}C/\gamma K^{36}C$ double mutant with $CuCl_2$

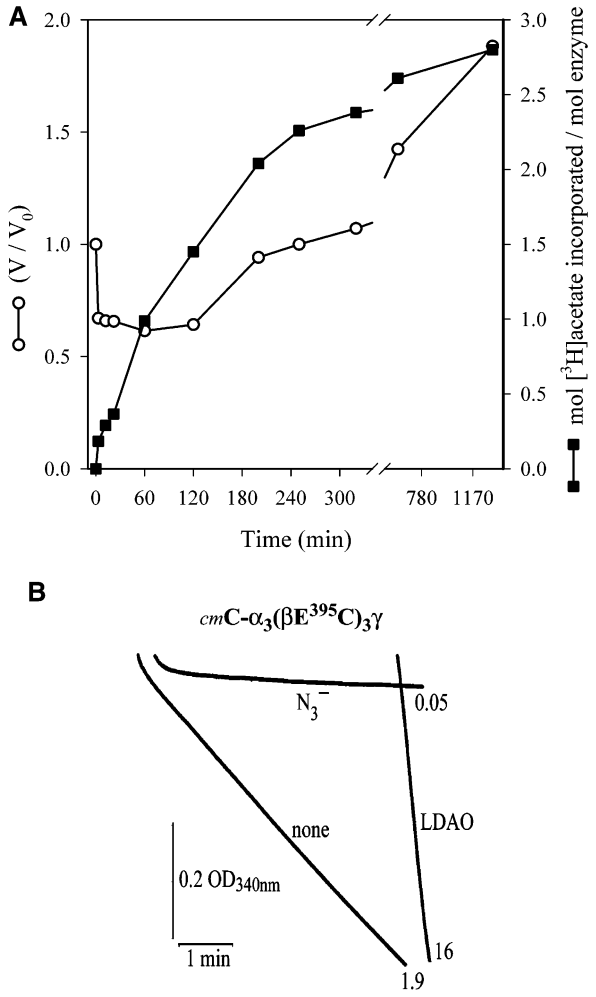

FIGURE 6: The effects of carboxymethylation of the introduced cysteines in the $\alpha_3(\beta E^{395}C)_3\gamma$ single mutant subcomplex. (A) Correlation of the biphasic response of ATPase activity of the reduced $\alpha_3(\beta E^{395}C)_3\gamma$ single mutant subcomplex with modification of the introduced cysteines. The reduced $\beta E^{395}C$ single mutant, at 1 mg/mL in 50 mM Tris-Cl, pH 8.0 containing 1 mM EDTA was treated with 4 mM iodo[^{3}H]acetate. At the times indicated by open circles, 10 μg samples were withdrawn and assayed for ATPase activity. At the times indicated by closed squares, 70 μL samples were withdrawn and passed through 1-mL centrifuge columns of Sephadex G-50 equilibrated with 50 mM Tris-Cl, pH 8.0 containing 0.1 mM EDTA to remove excess iodo[^{3}H]acetate. Protein concentrations and radioactivity in the column effluents were measured as described under Experimental Procedures. (B) The effects of azide and LDAO on the hydrolysis of 2 mM ATP catalyzed by the completely carboxymethylated single mutant enzyme (*cm*C-$\alpha_3(\beta E^{395}C)_3\gamma$). Assays were performed as described in the legend of Figure 4 using 5 μg of the modified single mutant in the presence and absence of 1 mM NaN3 or 0.06% LDAO. The number on the traces represent the final rates of ATP hydrolysis expressed in μmol of ATP hydrolyzed mg^{-1} min^{-1}. The numbers on the traces represent the final rates of ATP hydrolysis recorded in the last 30 s of each assay expressed in μmol of ATP hydrolyzed mg^{-1} min^{-1}.

confirms the suspicion of Ma et al. that the ionic track postulated to guide rotation of the γ subunit during catalysis might not fully apply to nonmitochondrial ATP synthases (*9*). In amino acid sequences of the γ subunit from over 70 different species obtained from the unique entries in Swiss-Prot/TrEMBL and GeBank, the position corresponding to γ^{36} in MF_1 is occupied by Lys or Arg in most mitochondrial F_1-ATPases listed. Notable exceptions are the γ subunits of the mitochondrial F_1-ATPases from two plant species, *Ipomoea batatas* (sweet potato) and *Arabidopsis thaliana.* The former contains Thr and the latter contains Gly in this position. It is interesting that both contain Arg in position 37. Although Lys occupies position 36 in the γ subunit of TF_1, position 36 is occupied by Asp in *E. coli* F_1-ATPase (EF_1) and Glu in chloroplast F_1-ATPase (CF_1), two other F_1-ATPases that have been thoroughly characterized (*18*, *19*).

The observation that $\beta-\gamma$ cross-links formed rapidly when the $\beta E^{395}C/\gamma R^{33}C$ and $\beta E^{395}C/\gamma R^{75}C$ double mutant subcomplexes of TF_1 were treated with $CuCl_2$ suggests that the side chains of γArg^{33} and γArg^{75} of TF_1 might be part of a modified ionic track in nonmitochondrial ATP synthases. Lys or Arg residues occupy position 33 in most of the over 70 sequences of the γ subunit from different species obtained from searching in Swiss-Prot/TrEMBL and GenBank. In contrast, position 33 is occupied by amino acids other than Lys or Arg in most of the nonmitochondrial F_1-ATPases listed. Again, notable exceptions are the γ subunits of the mitochondrial F_1-ATPases from *I. batatas* and *A. thaliana*, both of which contain Ala in position 33. However, both contain Arg in position 32.

When assayed in the presence of DTT, the steady-state ATPase activities of the mutant enzymes containing the $\beta E^{395}C$ substitution are 2−8% of the activity exhibited by the wild-type enzyme. Consistent with this observation, Hara et al. (*20*) reported that the ATPase activity of the $\alpha_3(\beta E^{395}A)_3\gamma$ subcomplex of TF_1 is about 3% the rate exhibited by the wild-type subcomplex. In an earlier study, it was demonstrated that the $\beta E^{395}A$ substitution had essentially no effect on torque generation during ATP-driven rotation of the γ subunit when immobilized single molecules of the mutant $\alpha_3\beta_3\gamma$ subcomplex hydrolyzed ATP (*21*). However, Hara et al. (*20*) provided convincing evidence indicating that the carboxylate of βE^{395} in TF_1 interacts with positively charged side chains in the C-terminal α-helix of the ϵ subunit when ϵ is in its inhibitory conformation (*22*).

The carboxylates in the side chains of Glu^{395} in β_{TP} and β_{DP} are 8.5 Å apart and are in the vicinity of the side chains of Ile^{390} in β_{TP} and β_{DP}, which, as pointed out by Tsunoda et al. (*16*), are in contact in crystal structures of MF_1. Therefore, it could be argued that, by eliminating a negatively charged side chain in ^{394}DELSEED^{400} segments in β subunits, the $\beta E^{395}C$ and $\beta E^{395}A$ substitutions might slow ATP hydrolysis by increasing the stability of transient β_{TP}/β_{DP} contacts during sequential firing of catalytic sites. However, the observation that carboxymethylation of all three introduced cysteines in the $\alpha_3(\beta E^{395}C)_3\gamma$ subcomplex only increases ATPase activity 2-fold is inconsistent with this argument.

The single and double mutants containing the $\beta E^{395}C$ substitution, including the carboxymethylated single mutant subcomplex are stimulated to a much greater extent by LDAO (7−25-fold) than the wild-type subcomplex (4.3-fold) and the $\gamma K^{36}C$, $R^{33}C$, and $R^{75}C$ singly substituted subcomplexes (3.8−4.7-fold). On the basis of the catalytic characteristics of other mutant $\alpha_3\beta_3\gamma$ subcomplexes of TF_1 (*23*), this indicates that subcomplexes containing the $\beta E^{395}C$ substitution have a greater propensity to entrap inhibitory MgADP in a catalytic site during turnover. Previous studies have shown that nucleotide-depleted MF_1 (*24*) and the nucleotide-depleted wild-type $\alpha_3\beta_3\gamma$ subcomplex of TF_1 (*14*) hydrolyze 50 μM ATP in three distinct phases: an initial

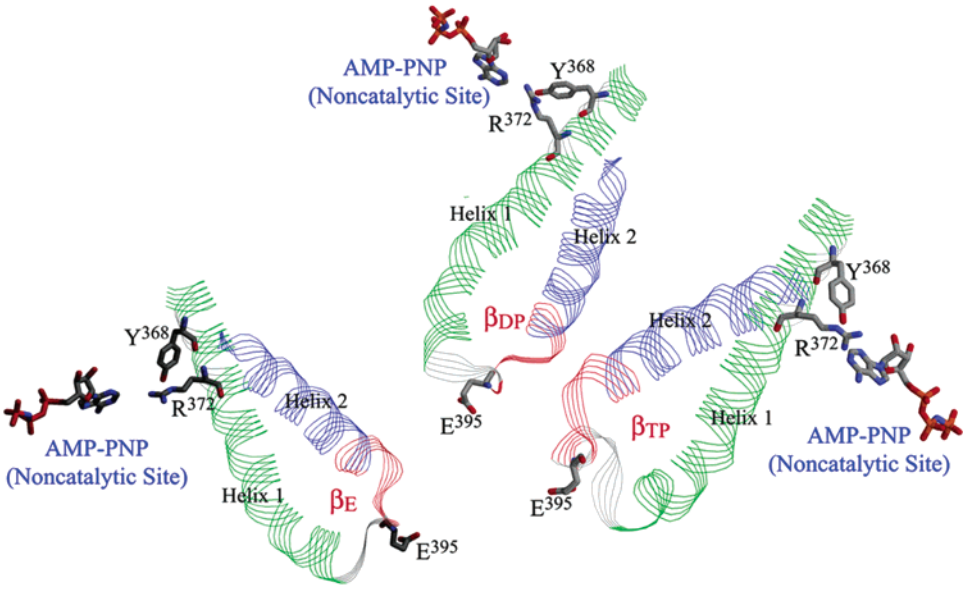

FIGURE 7: The helix−turn−helix motif in the C-terminal domains of β subunits in the original crystal structure of MF_1 (*2*). The three views of the helix−turn−helix motifs in β_E, β_{DP}, and β_{TP}, that include the side chains of βGlu^{395} in the turn, βArg^{372} and βTyr^{368} in helix 1, and AMP−PNP at the three noncatalytic nucleotide binding sites, were constructed individually using the RasMol software program provided by Roger Sayle (Glaxo Wellcome Research and Development, Greenford, United Kingdom) and were assembled with the Adobe Photoshop 5.0 program.

burst that rapidly decays into a slow intermediate phase, which, in turn, accelerates slowly into the final steady-state rate. After loading the high-affinity catalytic site of MF_1 and the wild-type $\alpha_3\beta_3\gamma$ subcomplex with MgADP, the enzymes hydrolyze 50 μM ATP with a slowly accelerating lag phase that closely resembles the transition from the intermediate phase to the final steady-state rate when the nucleotide-depleted enzymes hydrolyze 50 μM ATP. From these and other observations, it is generally accepted that the transition from the burst to the intermediate phase is caused by entrapment of MgADP in a catalytic site during turnover and that transition from the intermediate phase to the final rate is caused by slow binding of ATP to noncatalytic sites (*14*, *23*, *24*). The abrupt, biphasic behavior observed when the mutant subcomplexes containing the $\beta E^{395}C$ substitution hydrolyze 2 mM ATP in the absence of LDAO illustrated in Figure 4 suggests that turnover-dependent entrapment of inhibitory MgADP in a catalytic site is not relieved by the binding of ATP to noncatalytic sites. The slow steady-state activity observed with these mutant subcomplexes reflects the F_1·MgADP ⇆ F_1·MgADP* equilibrium described by Vasileva et al. (*25*) where F_1·MgADP* represents enzyme with MgADP bound to a catalytic site in an inhibitory mode and F_1·MgADP represents MgADP bound to a catalytic site in a noninhibitory mode.

In an earlier study, we demonstrated that the ATPase activity of the oxidized $(\alpha F^{357}C)_3(\beta R^{372}C)_3\gamma$ double mutant containing $\alpha-\beta$ cross-links at two noncatalytic site interfaces was stimulated 13-fold by LDAO, whereas the ATPase activity of the non-cross-linked double mutant was stimulated 5.7-fold by the detergent (*17*). In crystal structures of bovine MF_1, the ^{392}GMDELS^{397} segment is the turn in the helix−turn−helix motif in the C-terminal domain of β subunits. Figure 7 illustrates this motif in the three β subunits in the original crystal structure of bovine MF_1 (*2*). The side chain of βE^{395} protrudes from the loop near the center of the turn that connects helix 1 with helix 2 in all three β subunits. The side chains of βY^{368} and βR^{372} in helix 1 are near the adenines of AMP-PNP bound to noncatalytic sites in the crystal structures of MF_1. Modification of the equivalent of each of these residues in TF_1 affects the rate of ATP hydrolysis. Inactivation of five subunit TF_1 ($\alpha_3\beta_3\gamma\delta\epsilon$) with 5′-*p*-fluorosulfonyl[^{3}H]adenosine is caused by derivatization of the equivalent of βY^{368} in MF_1 (*26*). After cross-linking the introduced cysteines in the $(\alpha F^{357}C)_3(\beta R^{372}C)_3\gamma$ subcomplex of TF_1, the ATPase activity was reduced to 10% of the rate catalyzed by the wild-type subcomplex (*17*). Therefore, it is reasonable to assume that substitution of βE^{395} in the ^{392}GMDELS^{397} segment with Cys or Ala might affect the orientation of the α subunit with respect to the β subunit at the noncatalytic site interface, thereby altering the affinity of noncatalytic sites for nucleotides or affecting the conformational equilibrium between noncatalytic and catalytic sites.

REFERENCES

1. Yoshida, M., Muneyuki, E., and Hisabori, T. (2001) ATP synthase − a marvelous rotary engine of the cell. *Nat. Rev. Mol. Cell Biol. 2*, 669−677.
2. Abrahams, J. P., Leslie, A. G. W., Lutter, R., and Walker, J. E. (1994) Structure at 2.8 Å resolution of F_1-ATPase from bovine heart mitochondria. *Nature 370*, 621−628.
3. Braig, K., Menz, R. I., Montgomery, M. G., Leslie, A. G. W., and Walker, J. E. (2000) Structure of bovine heart mitochondrial F_1-ATPase inhibited by Mg^{2+} ADP and aluminum fluoride. *Structure 8*, 567−573.
4. Gibbons, C., Montgomery, M. G., Leslie, A. G. W., and Walker, J. E. (2000) The structure of the central stalk in bovine F1-ATPase at 2.4 Å resolution. *Nat. Struct. Biol. 7*, 1055−1061.
5. Menz, R. I., Walker, J. E., and Leslie, A. G. W. (2001) Structure of bovine mitochondrial F_1-ATPase with nucleotide bound to all three catalytic sites: implications for mechanism of rotary catalysis. *Cell 106*, 331−341.
6. Noji, H., Yasuda, R., Yoshida, M., and Kinosita, K., Jr. (1997) Direct observation of the rotation of F_1-ATPase. *Nature 386*, 299−302.
7. Yasuda, R., Noji, H., Kinosita, K., Jr., and Yoshida, M. (1998) F_1-ATPase is a highly efficient molecular motor that rotates with discrete 120° steps. *Cell 93*, 1117−1124.

8. Yasuda, R., Noji, H., Yoshida, M., Kinosita, K., Jr., and Itoh, H. (2001) Resolution of distinct rotational substeps by millisecond kinetic analysis of F_1-ATPase. *Nature 410*, 898−204.
9. Ma, J., Flynn, T. C., Cui, Q., Leslie, A. G. W., Walker, J. E., and Karplus, M. (2002) A dynamic analysis of the rotation mechanism for conformational change in F(1)-ATPase. *Structure 10*, 921−931.
10. Matsui, T., and Yoshida, M. (1995) Expression of wild-type and the Cys-/Trp-less $\alpha_3\beta_3\gamma$ complex of thermophilic F_1-ATPase in *Eschericia coli*. *Biochim. Biophys. Acta 1231*, 139−146.
11. Bandyopadhyay, S., Valder, C. R., Huynh, H. G., Ren, H., and Allison, W. S. (2002) The $\beta G^{156}C$ substitution in the F_1-ATPase from the thermophilic *Bacillus* PS3 affects catalytic cooperativity by destabilizing the closed conformation of the catalytic site. *Biochemistry 41*, 14421−14429.
12. Bradford, M. M. (1976) A rapid and sensitive method for the quantitation of microgram quantities of protein utilizing the principle of protein-dye binding. *Anal. Biochem. 72*, 248−254.
13. Penefsky, H. S. (1977) Reversible binding of P_i by beef heart mitochondrial adenosine triphosphatase. *J. Biol. Chem. 252*, 2891−2899.
14. Jault, J.-M., Matsui, T., Jault, F. M., Kaibara, C., Muneyuki, E., Yoshida, M., Kagawa, Y., and Allison, W. S. (1996) The $\alpha_3\beta_3\gamma$ complex of the F_1-ATPase from Thermophilic *Bacillus* PS3 containing the $\alpha D^{261}N$ substitution fails to dissociate inhibitory MgADP from a catalytic site when ATP binds to noncatalytic sites. *Biochemistry 34*, 16412−16418.
15. Matsui, T., Muneyuki, E., Honda, M., Allison, W. S., Dou, C., and Yoshida, M. (1997) Catalytic activity of the $\alpha_3\beta_3\gamma$ complex of F_1-ATPase without noncatalytic nucleotide binding site. *J. Biol. Chem. 272*, 8215−8221.
16. Tsunoda, S. P., Muneyuki, E., Amano, T, Yoshida, M, and Noji, H. (1999) Cross-linking of two beta subunits in the closed conformation in F_1-ATPase. *J. Biol. Chem. 274*, 5701−5706.
17. Bandyopadhyay, S., Ren, H., Wang, C. S., Allison, W. S. (2002) The $(\alpha F^{357}C)_3(\beta R^{372}C)_3\gamma$ subcomplex of the F_1-ATPase from the thermophilic *Bacillus* PS3 has altered ATPase activity after cross-linking α and β subunits at noncatalytic site interfaces. *Biochemistry 41*, 3226−3234.
18. Senior, A. E., Nadanaciva, S., and Weber, J. (2002) The molecular mechanism of ATP synthesis by F_1F_o-ATP synthase. *Biochim. Biophys. Acta 1553*, 188−211.
19. Frasch, W. D. (2000) The participation of metals in the mechanism of the F(1)-ATPase. *Biochim. Biophys. Acta 1458*, 310−325.
20. Hara, K. Y., Kato-Yamada, Y., Kikuchi, Y., Hisabori, T., and Yoshida, M. (2001) The role of the DELSEED motif of F_1-ATPase. *J. Biol. Chem. 276*, 23969−23973.
21. Hara, K. Y., Noji, H., Bald, D., Yasuda, R., Kinosita, K., and Yoshida, M. (2000) The role of the DELSEED motif of the β subunit in rotation of F_1-ATPase. *J. Biol. Chem. 275*, 14260−14263.
22. Tsunoda, S. P., Rodgers, A. J. W., Aggeler, R., Wilce, M. C. J., Yoshida, M., and Capaldi, R. A. (2001) Large conformational changes of the ϵ subunit in the bacterial F_1F_o ATP synthase oprovide a ratchet action to regulate this rotary motor enzyme. *Proc. Natl. Acad. Sci. U.S.A. 98*, 6560−6564.
23. Ren, H., and Allison, W. S. (2000) On What Makes the γ Subunit Spin during ATP Hydrolysis by F_1. *Biochim. Biophys. Acta 1458*, 221−233.
24. Jault, J.-M., and Allison, W. S. (1993) Slow Binding of ATP to Noncatalytic Nucleotide Binding Sites which Accelerates Catalysis Is Responsible for Apparent Negative Cooperativity Exhibited by the Bovine Mitochondrial F_1-ATPase. *J. Biol. Chem. 268*, 1558−1566.
25. Vasileva, E. A., Minkov, I. B., Fitin, A. F., and Vinogradov, A. D. (1980) Kinetic Mechanism of Mitochondrial Adenosine Triphosphatase. *Biochem. J. 202*, 9−14.
26. Bullough, D. A., Yoshida, M., and Allison, W. S. (1986) Sequence of the radioactive tryptic peptide obtained after inactivating the F_1-ATPase of the thermophilic bacterium PS3 with 5′-*p*-fluorosulfonylbenzoyl[^{3}H]adenosine at 65°. *Arch. Biochem. Biophys. 244*, 865−871.

BI036058I